

The quantum optical Josephson interferometer

Dario Gerace,^{1,2} Hakan E. Türeci,¹ A. Imamoglu,¹ Vittorio Giovannetti³ and Rosario Fazio^{3,4}

¹*Institute of Quantum Electronics, ETH Zurich, 8093 Zurich (Switzerland)*

²*CNISM and Dipartimento di Fisica "A. Volta," Università di Pavia, 27100 Pavia (Italy)*

³*NEST (CNR-INFN) and Scuola Normale Superiore, Piazza dei Cavalieri 7, 56126 Pisa (Italy)*

⁴*International School for Advanced Studies (SISSA), via Beirut 2 – 4, 34014 Trieste (Italy)*

The interplay between coherent tunnel coupling and on-site interactions in dissipation-free bosonic systems has led to many spectacular observations, ranging from the demonstration of number-phase uncertainty relation to quantum phase transitions. To explore the effect of dissipation and coherent drive on tunnel coupled interacting bosonic systems, we propose a device that is the quantum optical analog of a Josephson interferometer. It consists of two coherently driven linear optical cavities connected via a central cavity with a single-photon nonlinearity. The Josephson-like oscillations in the light emitted from the central cavity as a function of the phase difference between two pumping fields can be suppressed by increasing the strength of the nonlinear coupling. Remarkably, we find that in the limit of ultra-strong interactions in the center-cavity, the coupled system maps on to an effective Jaynes-Cummings system with a nonlinearity determined by the tunnel coupling strength. In the limit of a single nonlinear cavity coupled to two linear waveguides, the degree of photon antibunching from the nonlinear cavity provides an excellent measure of the transition to the nonlinear regime where Josephson oscillations are suppressed.

PACS numbers:

I. INTRODUCTION

Cavity quantum electrodynamics (QED) experiments based on strong coupling of a single anharmonic emitter to a cavity-mode have led to the observation of the photon blockade effect where photon-photon interactions alter the statistics of light emitted by the cavity. Experimental results showing nonlinearities at the single-photon level have recently been achieved in both atomic^{1,2} and solid-state QED systems^{3,4,5,6} with single cavities. Motivated by the success of single-cavity QED experiments, center of attention has now shifted to the exploration of the rich physics promised by strongly-correlated quantum optical systems in multi-cavity and extended photonic media. Several works have recently considered this possibility: a photonic version of the Bose-Hubbard model with an array of nonlinear cavities^{7,8,9}, the realization of the Tonks-Girardeau regime of interacting bosons in a non-linear optical fiber¹⁰, and a photonic analogue of the Kondo effect in a 1D waveguide¹¹. Most of the existing proposals have focused so far on strongly-correlated photonic systems in the quasi-equilibrium regime for which dissipation is essentially negligible. In most realistic cavity-QED structures on the other hand, dissipation does play a substantial role and it is very difficult to fix the photon number. When photon losses cannot be neglected, the system reaches a stationary state given by the balance of dissipation and driving. We propose here an optical analogue of the superconducting Josephson interferometer, which we name the *quantum optical Josephson interferometer*, revealing new features due to the genuine non-equilibrium interplay of coherent tunneling and on-site interactions.

The two variants of the device we are presenting couple a central nonlinear cavity to two external driving lasers

through either two side cavities (Fig. 1a,b) or two waveguides (Fig. 1d). The three-cavity system can be generalized to an N-cavity system with the central nonlinear one¹² (Fig. 1c), and in the limiting case of very large N this reduces to the single cavity coupled to two side-waveguides (Fig. 1d). In both cases, the coupling to the side cavities (or waveguides) is a consequence of photon tunneling. We assume the center-cavity can be tuned to have a sizable single-photon nonlinearity, e.g. due to some radiation-matter interaction effect, be it Jaynes-Cummings-type dynamics (with a single atom or quantum dot in the center cavity)¹³, giant Kerr nonlinearity¹⁴, or 0D polariton interaction (e.g., with a quantum well embedded in the center-cavity)¹⁵. The model discussed here is quite general and can be realized in a variety of quantum optical systems. In the following we show that light emitted from the center cavity is the result of two competing effects, tunneling and interactions, leading to a crossover between the coherent and strongly correlated regimes. In the coherent regime, photons are delocalized over the three cavities and the emitted light is strongly dependent on the phase difference between the two pumping lasers (Josephson oscillations). In the strongly correlated regime, the inhibition of photon number occupation beyond Fock states $|0\rangle$ and $|1\rangle$ in the center cavity reduces the quantum coherence between the two outer ones. The suppression of Josephson oscillations in the emitted light is accompanied by a crossover from Poissonian to sub-Poissonian photon statistics.

The main thrust of the present work is to investigate the crossover from coherent to correlated regimes of this intrinsically non-equilibrium system by detecting light emitted from the center cavity. We show that photon correlation measurements reveal features of an interacting few-body system that are not captured by more tra-

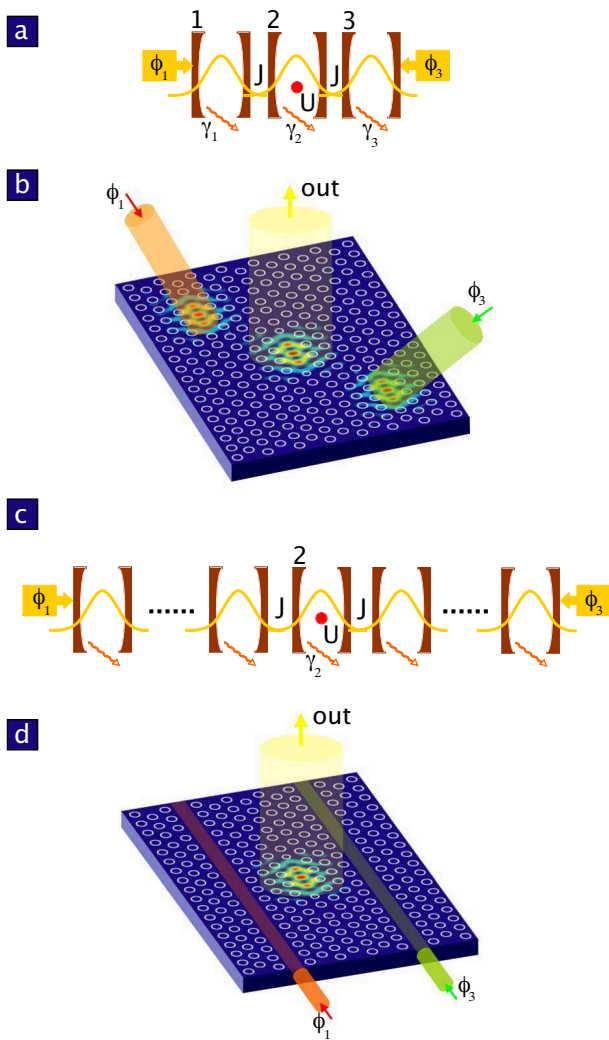


Figure 1: The systems under consideration. (a) Schematic of the quantum optical Josephson interferometer with three coupled cavities. The relevant quantities of the model are also defined. (b) A possible photonic crystal-based implementation (with calculated cavity mode profiles), where the middle cavity can contain a quantum dot or a quantum well in strong coupling with the high-Q photonic crystal cavity mode. (c) Schematic of an interferometer in the limit of a large number of coupled linear cavities in optical contact with the central nonlinear cavity, in which only the edges of the system are pumped. (d) A possible solid-state implementation of (c) employing a photonic crystal circuit with two side-waveguides coupled to the central nonlinear cavity.

ditional transport-type measurements. In fact, the device we propose has close analogies with a phase-biased Cooper pair transistor. In the latter, the critical current can be electrostatically modulated by changing the gate potential on the central island connected to two superconducting reservoirs^{16,17}. The interplay between coherent tunnel coupling and on-site interactions in these systems has been utilized in many ground-breaking ex-

periments, ranging from the observation of a quantum phase transition in Josephson junction arrays¹⁸ to the direct demonstration of number-phase uncertainty in superconducting islands¹⁹. While the operation of both electronic and photonic versions is based on the quantum mechanical conjugation between phase and number variables, the quantum optical Josephson interferometer is an intrinsically open system. Given the enormous impact of the Josephson devices in electronics, from metrology to quantum information processing, we expect that the quantum optical Josephson interferometer might constitute the building block for a new class of quantum optical devices.

II. THEORETICAL DISCUSSION

In the absence of losses the three cavity setup depicted in Fig. 1a,b is described by the Hamiltonian

$$\hat{H} = \sum_{k=1}^3 \Delta_k \hat{p}_k^\dagger \hat{p}_k + J(\hat{p}_1^\dagger \hat{p}_2 + \hat{p}_2^\dagger \hat{p}_3 + \text{h.c.}) + U \hat{p}_2^\dagger \hat{p}_2^\dagger \hat{p}_2 \hat{p}_2 + \sum_{k=1,3} (E_k \hat{p}_k^\dagger + \text{h.c.}), \quad (1)$$

written in the rotating frame with respect to the frequencies of the two pumping lasers ($\hbar = 1$). In the above equation, $\Delta_k = \omega_k - \omega_L$ are the detunings of the coherent pump lasers whose amplitudes are $E_{1,3} = |E_{1,3}| \exp\{i\phi_{1,3}\}$, where $|E_{1,3}|$ are assumed time-independent (cw pumping). We will characterize the three cavity system by analyzing the response of the center-cavity as a function of the phase difference $\phi = \phi_3 - \phi_1$. The two couplings J and U quantify the hopping strength between neighboring cavities and the nonlinear photon coupling in the center-cavity, respectively. The operators $\hat{p}_{1,3}$ describe noninteracting bosonic fields in the external cavities, i.e. free cavity photons, while the elementary excitations in the center-cavity are interacting polaritons denoted by \hat{p}_2 . Both the tunneling and the coherent pumping act on purely photonic degrees of freedom, e.g. J is due to the overlap of the photonic part among nearest neighbors cavities. A rigorous derivation of the model in Eq. (1) inevitably depends on the specific system under consideration, and has been provided before in the context of atomic⁷ or solid-state¹⁵ cavity-QED implementations. Readily accessible schemes for achieving large photon-photon interactions are based on resonant coupling of a single emitter to a cavity mode (i.e. the Jaynes-Cummings model). As we detail in the Supplementary Information section (“Experimental Feasibility”), the principal features we obtain using the model (1) are qualitatively identical to those predicted by the Jaynes-Cummings model-type single-photon nonlinearity.

The dynamics of the full model, Eq. (1), is effectively equivalent to that of two coupled bosonic fields: one is coherently driven, while the other is nonlinear (see Methods

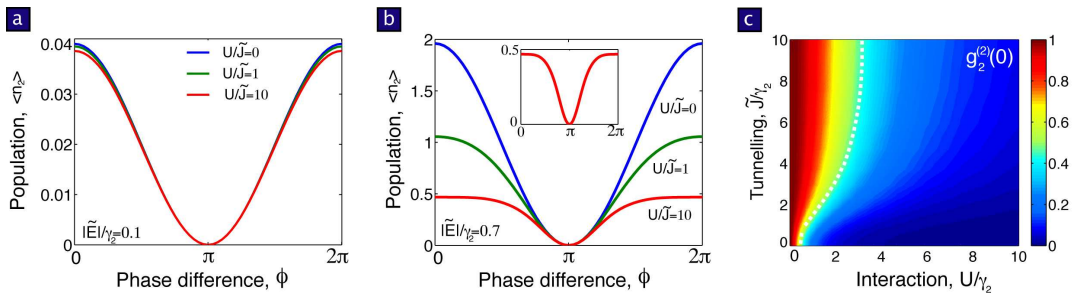


Figure 2: Numerical solutions for the three cavity system. (a) Average population in the center cavity as a function of ϕ for different values of U/\tilde{J} , in the weak pumping regime ($|\tilde{E}|/\gamma_2 = 0.1$): Josephson oscillations are barely modified as U is increased. (b) The same quantity as in (a), but in a stronger pumping regime ($|\tilde{E}|/\gamma_2 = 0.7$): Josephson oscillations are suppressed by increasing the interaction strength. The inset shows the curve calculated for $U/\tilde{J} = 10$. (c) Second-order correlation function as a function of \tilde{J} and U for $\gamma_1/\gamma_2 = 5$ under weak pumping conditions, $|\tilde{E}|/\gamma_2 = 0.1$, showing the transition from Poissonian (red) to sub-Poissonian (blue) light statistics. The functional dependence $U_{th}(\tilde{J})$ is highlighted with a dashed white line.

section). From now on we consider for simplicity the case of equal detunings and resonant pumping, $\Delta_k = \Delta = 0$. Losses can be taken into account within the quantum Master equation in Born-Markov approximation for the system density matrix ρ , which is expressed in the usual Lindblad form²². The relevant Master equation for this model is

$$\frac{\partial \rho}{\partial t} = i[\rho, \hat{H}] + \sum_{k=1}^3 \frac{\gamma_k}{2} (2\hat{p}_k \rho \hat{p}_k^\dagger - \hat{p}_k^\dagger \hat{p}_k \rho - \rho \hat{p}_k^\dagger \hat{p}_k). \quad (2)$$

In most of the relevant regimes, the Master equation has to be solved numerically. A description of the approach used in this work is presented in the Methods section. In the remaining of the text, we will assume $\gamma_{1,3} = \gamma$. With the specific experimental settings of Figs. 1b and d in mind, inter-cavity tunnel coupling $J \simeq 1$ meV²⁰, cavity quality factor $Q \simeq 10^5$, i.e. $\gamma \simeq 0.01$ meV in the optical/near-infrared domain²¹, and nonlinear to dissipation rate ratio $U/\gamma = 10$ (see Supplementary Information) can be realistically achieved, which makes the following theoretical analysis experimentally relevant.

It is instructive to first consider the case in which there is no interaction ($U = 0$), where an exact analytical solution for the steady state of Eq. (2) can be obtained. The case of equal amplitudes of the two driving lasers ($E_1 = E_3 = E$) and equal losses in the three cavities ($\gamma = \gamma_2$) captures all the essential details of the non-interacting case. In steady state the average number of photons in the central cavity $\langle n_2 \rangle = \langle \hat{p}_2^\dagger \hat{p}_2 \rangle$ is found to be

$$\langle n_2 \rangle = \frac{64J^2|E|^2}{(8J^2 + \gamma^2)^2} \cos^2 \frac{\phi}{2}. \quad (3)$$

This is an analog of Josephson oscillations, imprinted in the light emitted from the center-cavity, due to the interference between the two coherent driving fields. Two features of this solution are to be noticed for a comparison with the more interesting $U \neq 0$ situation treated

below. First, the size of the oscillations is maximized at $J \sim \gamma/2$, as a result of an interplay of dissipation and interference. Moreover, while $\langle n_2(\phi = 0) \rangle$ is suppressed and eventually goes to zero for $J \gg \gamma$, the oscillations keep a cosine-like behavior as a function of ϕ .

In Fig. 2, we present our numerical results for experimentally accessible observables of the system when the interaction is switched on ($U > 0$). Rescaled quantities \tilde{J} and \tilde{E} are defined for the effective two-cavity model as outlined in the Methods section. Do the Josephson oscillations in $\langle n_2(\phi) \rangle$, as measured by detecting the light emitted from the center cavity (Fig. 1b), remain intact? In Fig. 2a, we plot $\langle n_2(\phi) \rangle$ for various values of the interaction at a pumping strength of $|\tilde{E}|/\gamma_2 = 0.1$. The size as well as the functional form of the oscillations barely change as U/\tilde{J} is varied across a wide range of values, under these weak pumping conditions. This picture changes dramatically when we pump the system stronger, shown in Fig. 2b for $|\tilde{E}|/\gamma_2 = 0.7$. Here, the average population in the center-cavity can be sizeable and nonlinear effects are more pronounced. In contrast to the weak pumping case (Fig. 2a), the size of the oscillations is suppressed to a great extent as U is increased. Besides the strong suppression of visibility, Fig. 2b shows a dramatic deviation from the cosine-like functional form, Eq. (3), as U/\tilde{J} is increased from zero (the behavior for $U/\tilde{J} \gg 1$ is shown in the inset).

Next we investigate how this cross-over is reflected in the photon statistics of light emitted from the center cavity. For this, in Fig. 2c we plot the zero-time delay second-order correlation function $g_2^{(2)}(0)$ (See Methods section) as a function of the scaled quantities U/γ_2 and \tilde{J}/γ_2 . We find that $g_2^{(2)}(0)$ displays a sharp transition from Poissonian to sub-Poissonian light statistics as the interaction strength U is increased. The threshold for anti-bunched (sub-Poissonian) light generation, U_{th} , is a function of J . For $\tilde{J}/\gamma_2 \ll 1$, the anti-bunching threshold is $U_{th}(\tilde{J}) \sim \gamma_2$, while for $J/\gamma_2 \gg 1$,

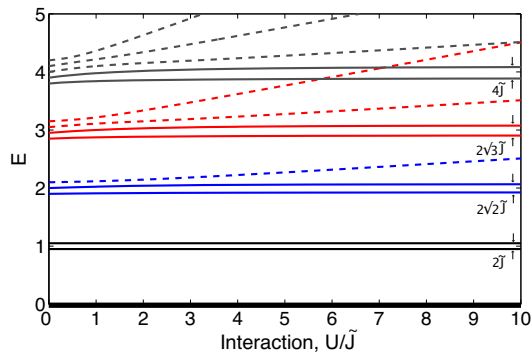


Figure 3: Variation of the energy levels of the three-cavity Josephson interferometer as a function of U/\tilde{J} . We plot the first few total photon number manifolds in the range $N_{tot} = 1$ to $N_{tot} = 4$, and $\tilde{J}/\gamma_2 = 0.05$. The various N_{tot} manifolds are marked on the vertical axis and set off from each other by an arbitrary ω_L for visibility. The energy levels in each manifold undergo an anticrossing at $U/\tilde{J} \sim 1$ and a crossover takes place to an effective Jaynes-Cummings sequence as $U/\tilde{J} \rightarrow \infty$.

$U_{th}(\tilde{J}) \sim \gamma + \gamma_2$. These two regimes are connected by a smooth crossover region. This peculiar behavior of the anti-bunching threshold is related to the effective dissipation rates of the coupled system as the coupling strength \tilde{J} is varied. At small \tilde{J} , the coupling to the center cavity is perturbative; the nonlinearity (i.e. antibunching) therefore sets in when U is larger than the broadening of the bare center cavity polariton states i.e. γ_2 . As \tilde{J} is increased, the coupling becomes non-perturbative and the relevant eigenstates of the coupled system are superpositions of center and outer cavity states; such dressed states have broadening contributions coming from both center and outer cavities and therefore the nonlinearity now has to be larger than the broadening of the dressed states in order for the system to exhibit antibunching. A remarkably simple expression for $g_2^{(2)}(0)$ can be derived in the weak pumping limit (See Discussion in Supplementary Information section) which captures all the regimes discussed:

$$g_2^{(2)}(0) = \frac{\Gamma^2}{\Gamma^2 + 4\alpha^2(\tilde{J})U^2}, \quad (4)$$

where $\Gamma = \gamma + \gamma_2$ and $\alpha(\tilde{J}) = (4\tilde{J}^2 + \gamma\Gamma)/(4\tilde{J}^2 + \gamma\gamma_2)$. These results are consistent with the expectation that strong photon nonlinearity can lead to photon-blockade¹⁴ in the center cavity giving rise to anti-bunching. While the *relative* strength of U with respect to tunnel coupling \tilde{J} seems to matter at small couplings \tilde{J}/γ_2 (i.e. $U_{th}(\tilde{J})$ is a monotonic function of \tilde{J}), at larger \tilde{J} the relative effect of U saturates.

An interesting feature that does not leave any footprint in these two observables considered is the nature of the system's effective non-linearity. For $U \ll \tilde{J}$, the devia-

tion of the system energy levels from a harmonic structure is linearly proportional to U , and this determines the main behaviour of $g_2^{(2)}(0)$. For $U \gg \tilde{J}$ however, the center cavity acts as a two-level system (only 0 and 1 photon states available), which is coupled to the linear cavities with strength \tilde{J} . Thus, the coupled system maps onto an effective Jaynes-Cummings (JC) model where, surprisingly, the tunnel coupling strength plays the role that is commonly played by the atom-cavity dipole-coupling in the original JC model¹³. In Fig. 3, we show how this comes about: two levels of each constant photon-number manifold ($N_{tot} = n_2 + n_s$) split off from the rest of the levels to form a JC-sequence as U is increased beyond \tilde{J} .

In the limit of an infinite number of linear cavities coupled on either side to the center cavity (Fig. 1c), we obtain a band of bosonic modes which mimic two external waveguides. The corresponding photon creation/annihilation operators in Eq. (1) can in this limit be replaced by their average (coherent state) values, $p_{1,3} \rightarrow \langle p_{1,3} \rangle = -2iE_{1,3}/\gamma$. The effective Hamiltonian of the system

$$\hat{H} \sim \Delta_2 \hat{p}_2^\dagger \hat{p}_2 + U \hat{p}_2^\dagger \hat{p}_2^\dagger \hat{p}_2 \hat{p}_2 + E_{\text{eff}} \hat{p}_2^\dagger + \text{h.c.}, \quad (5)$$

then reduces to that of a single nonlinear cavity pumped by a coherent field with amplitude $E_{\text{eff}} = -2iJ(E_1 + E_3)/\gamma$. We choose parameters such that $|E_{\text{eff}}| = J$, i.e. J acts as the effective pumping rate. The steady state results for $g_2^{(2)}(0)$ and $\langle n_2 \rangle$ are shown in Figs. 4a and 4b, respectively. The $g_2^{(2)}(0)$ displays a sharp transition from Poissonian to sub-Poissonian light statistics as the interaction strength U is increased. The threshold for anti-bunched (sub-Poissonian) light generation, U_{th} , is a function of J . For $J/\gamma_2 \ll 1$, the threshold is $U_{th} \sim \gamma_2$, in the opposite limit $U_{th} \sim J$. At small hoppings, the nonlinearity (i.e. anti-bunching) sets in when U is larger than the broadening of the bare center cavity polariton states i.e. γ_2 . Much more interesting is the fact that at larger hoppings the threshold scales with J , in contrast to the case of three cavities (Fig. 2c). The crossover from bunching to antibunching behavior reflects in a clear way the crossover from delocalized to localized states. As J is increased, the relevant eigenstates of the coupled system are superpositions of center and outer cavity states. When $J \gg U$ photon states are delocalized over the whole systems while in the opposite case the states are Fock states due to the onset of photon blockade. One may also understand the dependence of the crossover on J by relating it to the low- J limit of Fig. 2c: from the perspective of the center cavity, the driven waveguide is analogous to a driven cavity with a dissipation rate larger than all other energy scales.

Due to the Heisenberg uncertainty relation, the crossover from bunching to antibunching behavior manifests itself also in the phase dependence of $\langle n_2 \rangle$ shown in Fig. 4b. On increasing the interaction the visibility is strongly suppressed and furthermore there is a marked deviation from the simple cosine law found for $U = 0$.

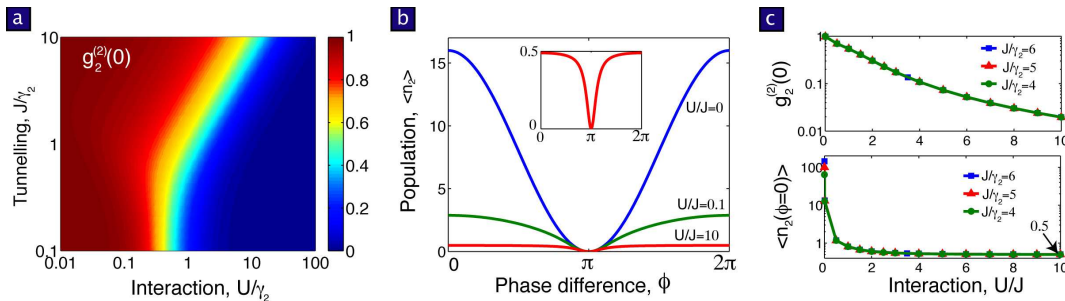


Figure 4: Numerical solutions for the waveguide-coupled limit. We assume the coherent states $|\langle p_{1,3} \rangle| = 1$. (a) Second-order correlation function at zero-time delay for light emitted from the center cavity, as a function of U and J . A sharp crossover between Poissonian (red) and sub-Poissonian (blue) statistics is seen in the $U - J$ plane. (b) Average population in the center cavity for $J/\gamma_2 = 2$ as a function of ϕ , for different values of U/J . The oscillations approach the limiting case of Eq. (6) when $U/J \gg 1$. The inset is a zoom on the curve for $U/J = 10$, showing $\langle n_2(\phi = 0) \rangle \rightarrow 0.5$ and a strong deviation from simple cosine-like behaviour. (c) Scaling of $g_2^{(2)}(0)$ and $\langle n_2(\phi = 0) \rangle$ as a function of U/J for different values of J/γ_2 , showing a smooth crossover from delocalized to localized regime for $U/J > 1$.

An analytical expression for the function in the inset can be found in the infinite- U limit, where Eq. (5) is replaced by a two-level system coupled with a driven cavity mode

$$\langle n_2 \rangle = \frac{\cos^2(\phi/2)}{2 \cos^2(\phi/2) + (\gamma^2/8J|E|)^2}, \quad (6)$$

which agrees with the numerical results. The broadening of the dip at $\phi = \pi$ is proportional to $\gamma^2/(4J|E|)$ implying that the visibility goes to zero by increasing the field ($\langle n_2(\phi = 0) \rangle \rightarrow 0.5$). The behavior of $\langle n_2(\phi) \rangle$ is again witness of the crossover from the delocalized to the correlated regimes. For large hopping the state of the system is approximately a coherent state. Phases are locked (there are strong fluctuations in the number operator) and the visibility is large. On the opposite case, due to photon blockade the state is close to a Fock state. Phase fluctuations in the central cavity suppress the global coherence of the system and the visibility is suppressed. We note that although the functional forms are different, both $\langle n_2(\phi = 0) \rangle$ and $g_2^{(2)}(0)$ display a cross-over that is dependent only on the dimensionless ratio U/J , as shown in Fig. 4c.

III. SUMMARY

In conclusion, we have studied the out-of-equilibrium interplay of tunneling and interactions in realistic quantum optical devices. For the three-cavity system, the inhibition of particle number fluctuations beyond Fock states $|0\rangle$ and $|1\rangle$ in the center-cavity reduces quantum coherence between the two outer ones. This is found to exhibit a threshold behavior as a function of the correlation energy U , which is clearly discernible from the saturation of Josephson oscillations at amplitude $\langle n_2 \rangle = 0.5$, and by a strong deviation from cosine-like behavior at strong pumping. Remarkably, we find that the effective non-linearity of the system displays a cross-over

into a JC-like non-linearity as U/J is increased beyond 1. Photon correlation measurements for this device reveal a sharp threshold from Poissonian to sub-Poissonian statistics that is almost insensitive to the strength of the tunnel-coupling J . On the other hand, in the case of a linear array of cavities coupled to a non-linear center cavity, the anti-bunching threshold is found to depend strongly on the tunnel-coupling. This observation signifies that photon correlation measurements are very effective in revealing the interplay of coherent tunneling and on-site interactions and may contain the key to interpret and probe possible phases of extended cavity-arrays which operate under non-equilibrium conditions.

IV. METHODS

The model in Eq. (1) is reformulated by introducing the canonically transformed bosonic operators $\hat{s} = (\hat{p}_1 + \hat{p}_3)/\sqrt{2}$ and $\hat{d} = (\hat{p}_1 - \hat{p}_3)/\sqrt{2}$, from which

$$\hat{H}_s = \Delta(\hat{s}^\dagger \hat{s} + \hat{p}_2^\dagger \hat{p}_2) + \tilde{J}(\hat{p}_2^\dagger \hat{s} + \hat{s}^\dagger \hat{p}_2) + U \hat{p}_2^\dagger \hat{p}_2^\dagger \hat{p}_2 \hat{p}_2 + \tilde{E} \hat{s}^\dagger + \tilde{E}^* \hat{s}, \quad (7)$$

where we defined $\Delta_k = \Delta$ and we discarded the dynamics of the field \hat{d} , which is decoupled from \hat{p}_2 . Rescaled quantities are defined as $\tilde{J} = \sqrt{2}J$ and $\tilde{E} = \sqrt{2}(E_1 + E_3)/2$. Thus, the dynamics of the full model (1) is equivalent to that of two coupled bosonic fields: \hat{s} is coherently driven, while \hat{p}_2 is nonlinear. Losses are taken into account within the quantum master equation in Born-Markov approximation for the system density matrix, Eq. (2), for the field operators \hat{s} and \hat{p}_2 with dissipations γ and γ_2 , respectively.

Analytical solution. An analytical solution to the steady state master equation can be found in the non-interacting limit, $U = 0$. The equation of motion for a generic operator expectation value, $\langle \hat{A} \rangle$, is $\partial \langle \hat{A} \rangle / \partial t = 0 = i \langle [\hat{H}_s, \hat{A}] \rangle_{ss} + \langle \mathcal{L}[\hat{A}] \rangle_{ss}$, where $\hat{H}_s = (\tilde{J}\hat{p}_2 + \tilde{E})\hat{s}^\dagger + \text{h.c.}$,

and the Liouvillian $\mathcal{L}[\hat{A}]$ is formally written as

$$\mathcal{L}[\hat{A}] = \frac{\gamma}{2}(2\hat{s}^\dagger\hat{A}\hat{s} - \hat{s}^\dagger\hat{s}\hat{A} - \hat{A}\hat{s}^\dagger\hat{s}) + \frac{\gamma_2}{2}(2\hat{p}_2^\dagger\hat{A}\hat{p}_2 - \hat{p}_2^\dagger\hat{p}_2\hat{A} - \hat{A}\hat{p}_2^\dagger\hat{p}_2). \quad (8)$$

Solving for \hat{p}_2 and \hat{s} , respectively, we get a system of two coupled equations, from which the steady state solution is $|\langle\hat{p}_2\rangle_{\text{ss}}| = |\bar{E}|/\{\bar{J}[(1 + \gamma\gamma_2/(4\bar{J}^2))]\}$, and hence Eq. (3).

Numerical solution. Extensive numerical simulations for the effective model (7) can be performed quite efficiently and in a reduced Hilbert space with respect to the full model. After explicitly defining the operators in matrix form on a Fock basis of bosonic number states, the steady state density matrix for any given set of parameters can be obtained by finding the eigenvector corresponding to the zero eigenvalue of the linear operator equation $\hat{L}|\rho\rangle\rangle = \lambda|\rho\rangle\rangle$, where $|\rho\rangle\rangle$ is the density operator mapped into vectorial form, and \hat{L} is the linear matrix corresponding to the Liouvillian operator in the right-hand side of Eq. (2)^{23,24}. Once $|\rho_{\text{ss}}\rangle\rangle$ is obtained from $\hat{L}|\rho\rangle\rangle_{\text{ss}} = \lambda_{\text{ss}}|\rho\rangle\rangle_{\text{ss}}$ with $\lambda_{\text{ss}} = 0$, we can recast it in matrix form and calculate any observable we are interested in. In particular, in this work we deal with $\langle n_2 \rangle = \text{Tr}\{\hat{p}_2^\dagger\hat{p}_2\rho_{\text{ss}}\}$, and the steady state zero-time delay second-order correlation function $g_2^{(2)}(\tau = 0) = \text{Tr}\{\hat{p}_2^\dagger\hat{p}_2^\dagger\hat{p}_2\hat{p}_2\rho_{\text{ss}}\}/\langle n_2 \rangle^2$. To check convergence with the number of Fock states in the basis as a function of \bar{J} , numerical results for $U = 0$ are compared to Eq. (3).

V. SUPPLEMENTARY INFORMATION

Experimental feasibility. In the main text we have considered a generic Kerr nonlinearity as the source of strong photon correlation in the center cavity. A possible way of experimentally implementing an effective hamiltonian of the type (1) or (5) in the main text is to couple 4-level atomic ensembles with microtoroid resonators, as described in detail in the literature⁷. The latter certainly represents an interesting possibility for a practical realization of our proposal with state-of-the art atomic cavity QED. Our focus here will be on the scheme represented in Fig. 1b and d (see text), in which a quantum dot (QD) is assumed to be deterministically coupled to the high-Q photonic crystal cavity mode in the middle⁴. It has been experimentally shown that such a system displays single-photon nonlinearities under coherent resonant pumping⁶. Photonic crystal (PC) circuits allow for a straightforward on-chip implementation with side-coupled cavities (as in Fig. 1b) or waveguides (as in Fig. 1d). If the hopping parameter J is small compared to the laser intensities $|E_1|$ and $|E_3|$, we can approximate the states of the external cavities with coherent fields of intensity $2|E_{1,3}|/\gamma$ (with γ being the damping parameter of the external cavities). Thus, to first order in $J/|E_{1,3}|$, the dynamics of the central cavity can be effectively described by replacing in the Hamiltonian the operators \hat{p}_1 and \hat{p}_3 with $2|E_{1,3}|/\gamma$, with reference to the derivation of the model in Eq. (5)

in the text. With this choice the 3-cavity set-up can be effectively reduced to a Jaynes-Cummings model coupled to external driving fields and described by the simplified model

$$\hat{H} \sim \Delta_c \hat{a}_2^\dagger \hat{a}_2 + \Delta_x \hat{\sigma}_+ \hat{\sigma}_- + ig(\hat{a}_2^\dagger \hat{\sigma}_- - \hat{\sigma}_+ \hat{a}_2) + E_{\text{eff}} \hat{a}_2^\dagger + E_{\text{eff}}^* \hat{a}_2, \quad (9)$$

where \hat{a}_2 (\hat{a}_2^\dagger) represents annihilation (creation) of cavity photons, while $\hat{\sigma}_-$, and $\hat{\sigma}_+$ are Pauli lowering and rising operators related to the effective two-level system representing the QD exciton transition; $g = \hbar(\pi e^2 f / \varepsilon m^* V_{\text{eff}})^{1/2}$ is the exciton-photon coupling (expressed in terms of the effective cavity mode volume and the QD oscillator strength)²⁵, and $\Delta_c = \omega_c - \omega_L$ and $\Delta_x = \omega_x - \omega_L$ are the cavity and exciton detuning from the pump frequency, respectively. The effective pumping strength is $|E_{\text{eff}}| \propto |E_1 + E_2|/\gamma$ and is responsible for the effects of phase detuning, $\phi = \phi_1 - \phi_3$.

To give some numbers, state-of-the art solid state QED with GaAs-based materials allows for $Q \sim 10^5 - 10^6$, i.e. realistic $\gamma_c \sim 0.01$ meV²¹, $\gamma_x \sim 1.3 \times 10^{-3}$ meV²⁶, $g = 0.11$ meV⁴. In the experiment, g is fixed as well as J , but the effective single-photon nonlinearity can be tuned by changing $\delta = \omega_x - \omega_c$. There are a number of different techniques to deterministically tune the cavity mode frequency^{4,27,28,29} and/or the QD exciton resonance³⁰. For the system excitation, the same laser source can be sent through a beam-splitter, one of the arms going directly into the PC circuit (e.g. through a tapered access waveguide) with phase ϕ_1 , while the other being delayed and sent through a second tapered waveguide into the circuit with phase ϕ_3 . Given that lasers with sub-MHz linewidth (i.e. much smaller than cavity and exciton dissipation rates) are currently available, we do not regard possible phase fluctuations in the two driving fields as a limiting issue for this scheme to be realized. Finally, it is key to this experiment that the pump laser frequencies be tuned to the lower polariton frequency of the JC spectrum, i.e. for each detuning δ we set $\omega_L \simeq (\omega_x + \omega_c)/2 - \sqrt{g^2 + \delta^2}/4^4$.

We simulate this model by solving the corresponding master equation that incorporates realistic cavity and exciton dissipation rates. Figure 5 shows that the predictions of the Jaynes-Cummings model in Eq. (9) are qualitatively similar to the ideal Kerr nonlinearity model of Eq. (5) in the main text. In particular, the dependence of light intensity on ϕ shows suppression of Josephson-like oscillations as the exciton frequency is tuned (from the blue-side) in resonance with the cavity mode. The increase of oscillations amplitude towards the bare-cavity limit appears together with a crossover from sub-Poissonian to Poissonian statistics as a function of δ , consistent with the results of Fig. 4 in the main text. Here, tuning δ is a way of effectively tuning the nonlinearity in the central cavity, and thereby to experimentally observe the crossover from tunnel-coupled to strong correlated photon dynamics in a state-of-the art device. Notice that the linear regime is completely recovered for

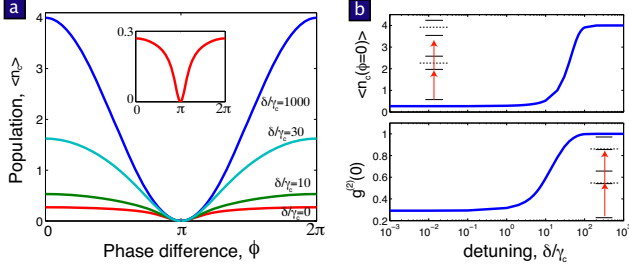


Figure 5: Numerical simulation of the experimental feasibility. We assume parameters of the model in Eq. (9) $g/\gamma_c = 10$, $g/\gamma_x = 100$ (as realistically achievable, see text), and effective pumping strength $|E_{\text{eff}}|/\gamma_c = 1$ at $\phi = 0$. Results are shown for light intensity and second-order correlation function emitted from the middle cavity, i.e. $\langle n_c \rangle = \langle \hat{a}_2^\dagger \hat{a}_2 \rangle$ and $g^{(2)}(0) = \langle \hat{a}_2^\dagger \hat{a}_2^\dagger \hat{a}_2 \hat{a}_2 \rangle / \langle n_c \rangle^2$. (a) Josephson-like oscillations are suppressed when the cavity-exciton detuning $\delta \rightarrow 0$. When $\delta \gg \gamma_c, g$, i.e. the exciton resonance is strongly blue-detuned from the cavity mode, the lower polariton is more and more cavity-like, hence the effective nonlinearity of the system is tuned through δ . In the inset, a zoom on the curve for $\delta = 0$. (b) The crossover from correlated to delocalized regimes is shown for $\langle n_c \rangle$ and $g^{(2)}(0)$ at $\phi = 0$, respectively, as a function of δ .

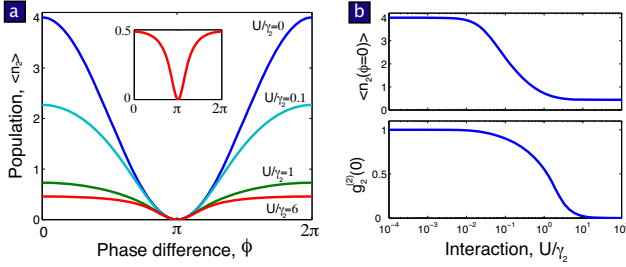


Figure 6: Numerical simulation for the model of Eq. (5) in the main text with effective pumping strength $|E_{\text{eff}}|/\gamma = 1$ at $\phi = 0$. (a) Josephson-like oscillations are suppressed on increasing the effective Kerr nonlinearity, U/γ_2 . In the inset, a zoom on the curve for $U/\gamma_2 = 6$, to be compared to the previous figure. (b) Crossover from correlated to delocalized regimes for $\langle n_2 \rangle$ and $g_2^{(2)}(0)$ at $\phi = 0$, respectively, as a function of U/γ_2 .

$\delta/\gamma_c \simeq 100$, i.e. $\delta \sim 1$ meV with the parameters given above, which is perfectly within reach of present experimental capabilities. In order to compare the behaviour of the different models, we notice that the strongly correlated limit of Fig. 5a ($\delta = 0$, curve in the inset) is qualitatively similar to the result obtained with a Kerr nonlinear model, Eq. (5) in the text, for $U = (2 - \sqrt{2})g$, i.e. $U/\gamma_2 \simeq 6$, as it is shown in Fig. 6a and its inset. The crossover from delocalized to localized regimes as a function of U is shown in Fig. 6b to be compared to Fig. 5b. The strict analogies between the experimental realization proposed and the model considered in the main text before is maintained as long as the pumping strength of

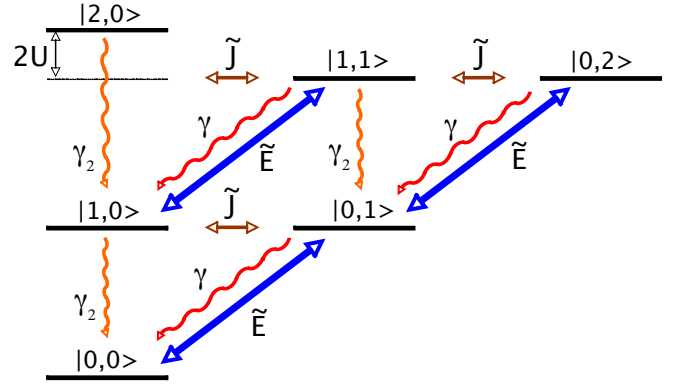


Figure 7: Energy level diagram and rates for the coupled cavity system. The various N_{tot} manifolds are set off from each other by an arbitrary ω_p for visibility. The numbering of the states $|n\rangle$ are from down to up and left to right. For instance $|1\rangle = |1,0\rangle$.

the Jaynes-Cummings system is low enough to discard higher-lying photon manifolds.

Finally, we stress that the same model and experimental approach can be used to study the realization of quantum optical Josephson interferometers based on different technologies, such as circuit QED³. Moreover, we point out again that the effective Kerr nonlinearity can be achieved, in the same system represented in Figs. 1b and d in the text, with a QW in strong coupling to the cavity mode. Although there is no experimental evidence of Kerr nonlinear behaviour of 3D confined cavity polaritons at time of writing, it is likely that polariton blockade on a single quantum box can be achieved in the near future along the lines and numbers quoted in the literature¹⁵, e.g. with an alternative cavity geometry recently realized³¹. Such a result would make possible a more direct realization of our model with a Kerr nonlinearity in the solid state.

Derivation of Eq. (4). Here we investigate the steady state dynamics of the Hamiltonian (7) (see Methods section, main text) in the weak pumping limit. We will present a derivation of the expressions for $\langle n_2(\phi = 0) \rangle$ and $g_2^{(2)}(\tau = 0) = \langle \hat{p}_2^\dagger \hat{p}_2^\dagger \hat{p}_2 \hat{p}_2 \rangle / \langle n_2 \rangle^2$. Consider the low-energy excitations of the Hamiltonian (7) in the basis $|n_2, n_s\rangle$ where $N_{\text{tot}} = n_2 + n_s$ is the total number of photons. In the weak pumping limit, the drive term $\tilde{E} \hat{s}^\dagger + \tilde{E}^* \hat{s}$ causes transitions between the manifolds N_{tot} and $N_{\text{tot}} + 1$. Let us write the total time-dependent wavefunction of the system as $\Psi(t) = \sum_n a_n |n\rangle$. In the weak pumping limit, we consider the lowest three total photon manifolds $N_{\text{tot}} = 0, 1, 2$, hence $n = 0, \dots, 6$. The corresponding energy level diagram and the rates are shown in Fig. 7.

Terms neglected in $\Psi(t)$ will be of order $O(\frac{\tilde{E}}{\tilde{\gamma}})^3$ where $\tilde{\gamma}$ is the typical decay rate of the system (γ_2, γ). It's important to write the equations of motion in the bare

basis instead of the basis of the coupled cavity states to get the dissipation rates correctly. The equations of motion are

$$\begin{aligned}
\dot{\tilde{a}}_0 &= 0 \\
\dot{\tilde{a}}_1 &= -\left(i\Delta + \frac{\gamma_2}{2}\right)\tilde{a}_1 - i\tilde{J}\tilde{a}_2 \\
\dot{\tilde{a}}_2 &= -\left(i\Delta + \frac{\gamma}{2}\right)\tilde{a}_2 - i\tilde{J}\tilde{a}_1 - i\tilde{E}\tilde{a}_0 \\
\dot{\tilde{a}}_3 &= -(2i\Delta + 2iU + \gamma_2)\tilde{a}_3 - i\sqrt{2}\tilde{J}\tilde{a}_4 \\
\dot{\tilde{a}}_4 &= -\left(2i\Delta + \frac{\Gamma}{2}\right)\tilde{a}_4 - i\sqrt{2}\tilde{J}(\tilde{a}_3 + \tilde{a}_5) - i\tilde{E}\tilde{a}_1 \\
\dot{\tilde{a}}_5 &= -(2i\Delta + \gamma)\tilde{a}_5 - i\sqrt{2}\tilde{J}\tilde{a}_4 - i\tilde{E}\tilde{a}_2
\end{aligned}$$

We have kept terms that are the same order of magnitude in $\frac{|\tilde{E}|}{\gamma}$ and $\tilde{a}_n = a_n e^{i\omega_L t}$ ³². The steady-state solutions can be easily determined by additionally employing the normalization condition $\sum_{n=1}^6 |a_n|^2 = 1$ (to order $O(\frac{|\tilde{E}|}{\gamma})^6$). We find, for $\Delta = 0$,

$$a_1 = -\frac{4\tilde{J}\tilde{E}}{\gamma\gamma_2 + 4\tilde{J}^2}, \quad a_2 = -\frac{2i\tilde{E}\gamma_2}{\gamma\gamma_2 + 4\tilde{J}^2} \quad (10)$$

It's interesting to note that in the limit $J/\gamma \gg 1$, $|a_1| \gg |a_2|$, showing that interference effects play an important role. Thus,

$$n_p \sim |a_1|^2 = 16\tilde{J}^2\tilde{E}^2/(\gamma\gamma_2 + 4\tilde{J}^2)^2 \quad (11)$$

to order $O(\frac{|\tilde{E}|}{\gamma})^4$. Solving for the two-photon manifold amplitudes as well, we find (4)

$$g_2^{(2)}(\tau = 0) \sim \frac{2|a_3|^2}{|a_1|^4} = \frac{\Gamma^2}{\Gamma^2 + 4\alpha^2(\tilde{J})U^2} \quad (12)$$

Acknowledgments

The authors would like to acknowledge useful discussions with I. Carusotto, C. Ciuti, and S. De Liberato. This work was partly supported by NCCR Quantum Photonics. R.F. acknowledges financial support from EUROSQIP. Correspondence and requests for materials should be addressed to D.G. (email: gerace@fisicavolta.unipv.it).

-
- ¹ Birnbaum, K. M. *et al.* Photon blockade in an optical cavity with one trapped atom. *Nature* **436**, 87-90 (2005).
 - ² Schuster, I. *et al.* Nonlinear spectroscopy of photons bound to one atom. *Nature Physics* **4**, 382-385 (2008).
 - ³ Schuster, D. I. *et al.* Resolving photon number states in a superconducting circuit. *Nature* **445**, 515-518 (2007).
 - ⁴ Hennessy, K. *et al.* Quantum nature of a strongly coupled single quantum dot-cavity system. *Nature* **445**, 896-899 (2007).
 - ⁵ Srinivasan, K. and Painter, O. Linear and nonlinear optical spectroscopy of a strongly coupled microdisk-quantum dot system. *Nature* **450**, 862-865 (2007).
 - ⁶ Faraon, A. *et al.* Coherent generation of nonclassical light on a chip via photon-induced tunneling and blockade. *Nature Physics* **4**, 859-863 (2008).
 - ⁷ Hartmann, M. J., Brandao, F. G. S. L. and Plenio, M. B. Strongly interacting polaritons in coupled arrays of cavities. *Nature Physics* **2**, 849-855 (2006).
 - ⁸ Greentree, A. D., Tahan, C., Cole, J. H. and Hollenberg, L. C. L. Quantum phase transitions of light. *Nature Physics* **2**, 856-861 (2006).
 - ⁹ Angelakis, D. G., Santos, M. F. and Bose, S. Photon-blockade-induced Mott transitions and XY spin models in coupled cavity arrays. *Phys. Rev. A* **76**, R031805 (2007).
 - ¹⁰ Chang, D. E. *et al.* Crystallization of strongly interacting photons in a nonlinear optical fibre. *Nature Physics* **4**, 884-889 (2008).
 - ¹¹ Shen, J. T. and Fan, S. Strongly correlated two-photon transport in a one-dimensional waveguide coupled to a two-level system. *Phys. Rev. Lett.* **98**, 153003 (2007).
 - ¹² Zhou, L., Gong, Z. L., Liu, Y., Sun, C. P. and Nori, F. Controllable scattering of a single photon inside a one-dimensional resonator waveguide. *Phys. Rev. Lett.* **101**, 100501 (2008).
 - ¹³ Jaynes, E. T. and Cummings, F. W. Comparison of quantum and semiclassical radiation theory with application to the beam maser. *Proc. IEEE* **51**, 89-109 (1963).
 - ¹⁴ Werner, M. J. and Imamoglu, A. Photon-photon interactions in cavity electromagnetically induced transparency. *Phys. Rev. A* **61**, R011801 (2000).
 - ¹⁵ Verger, A., Ciuti, C. and Carusotto, I. Polariton quantum blockade in a photonic dot. *Phys. Rev. B* **73**, 193306 (2006).
 - ¹⁶ Averin, D. V. and Likharev, K. K. in *Mesoscopic Phenomena in Solids*, ed. by Altshuler, B. L., Lee, P. A., and Webb, R. A. (North Holland, Amsterdam, 1991), p. 213.
 - ¹⁷ Matveev, K. A., Gisselält, M., Glazman, L. I., Jonson, M. and Shekhter, R. I. Parity-induced suppression of the Coulomb blockade of Josephson tunneling. *Phys. Rev. Lett.* **70**, 2940-2943 (1993).
 - ¹⁸ Geerligs, L. J., de Groot, L. E. M., Verbruggen, A. and Mooji, J. E. Charging effects and quantum coherence in regular Josephson junction arrays. *Phys. Rev. Lett.* **63**, 326-329 (1989).
 - ¹⁹ Elion, W. J., Matters, M., Geigenmüller, U. and Mooji, J. E. Direct demonstration of Heisenberg uncertainty principle in a superconductor. *Nature* **371**, 594-595 (1994).
 - ²⁰ Atlasov, K. A., Karlsson, K. F., Rudra, A., Dwir, B. and Kapon, E. Wavelength and loss splitting in directly coupled photonic-crystal defect microcavities. *Opt. Express* **16**, 16255-16264 (2008).
 - ²¹ Combrié, S., De Rossi, A., Tran, Q. V. and Benisty, H. GaAs photonic crystal cavity with ultrahigh Q: microwatt nonlinearity at 1.55 μm . *Opt. Lett.* **33**, 1908-1910 (2008).
 - ²² Carmichael, H. *An open systems approach to quantum optics* (Springer-Verlag, Berlin, 1993).
 - ²³ Jakob, M. and Stenholm, S. Variational functions in driven open quantum systems. *Phys. Rev. A* **67**, 032111 (2003).

- ²⁴ Diehl, S. *et al.* Quantum states and phases in driven open quantum systems with cold atoms. *Nature Physics* **4**, 878-883 (2008).
- ²⁵ Andreani, L. C., Panzarini, G. & Gerard, J.-M. Strong-coupling regime for quantum boxes in pillar microcavities: Theory. *Phys. Rev. B* **60**, 13276-13279 (1999).
- ²⁶ Vamivakas, N. *et al.* Strong extinction of a far-field laser beam by a single quantum dot. *Nano Lett.* **7**, 2892-2896 (2007).
- ²⁷ Badolato, A. *et al.* Deterministic coupling of single quantum dots to single nanocavity modes. *Science* **308**, 1158 (2005).
- ²⁸ Strauf, S. *et al.* Frequency control of photonic crystal membrane resonators by monolayer deposition. *Appl. Phys. Lett.* **88**, 043116 (2006).
- ²⁹ Hennessy, K., Högerle, C., Hu, E., Badolato, A. & Imamoglu, A. Tuning photonic nanocavities by atomic force microscope nano-oxidation. *Appl. Phys. Lett.* **89**, 041118 (2006).
- ³⁰ Rastelli, A. *et al.* In situ laser microprocessing of single self-assembled quantum dots and optical microcavities. *Appl. Phys. Lett.* **90**, 73120 (2007).
- ³¹ El Daïf, O. *et al.* Polariton quantum boxes in semiconductor microcavities. *Appl. Phys. Lett.* **88**, 061105 (2006).
- ³² The Hamiltonian in Equation (7) in the main text is written in the interaction picture. Here the wavefunction Ψ is the wavefunction written in the Schrödinger picture for completeness.